JACS
JOURNAL OF THE AMERICAN CHEMICAL SOCIETY
pubs.acs.org/JACS
Article

Calix[4]arene-Functionalized Titanium-Oxo Compounds for Perceiving Differences in Catalytic Reactivity Between Mono- and Multimetallic Sites

Ning Li,[§] Jiao-Min Lin,[§] Run-Han Li,[§] Jing-Wen Shi, Long-Zhang Dong, Jiang Liu, Jun He,* and Ya-Qian Lan*

Cite This: https://doi.org/10.1021/jacs.3c04480
Read Online

ABSTRACT: While the difference in catalytic reactivity between mono- and multimetallic sites is often attributed to more than just the number of active sites, still few catalyst model systems have been developed to explore more underlying causal factors. In this work, we have elaborately designed and constructed three stable calix[4]arene (C4A)-functionalized titanium-oxo compounds, **Ti-C4A**, **Ti_4-C4A**, and **Ti_{16}-C4A**, with well-defined crystal structures, increasing nuclearity, and tunable light absorption capacity and energy levels. Among them, **Ti-C4A** and **Ti_{16}-C4A** can be taken as model catalysts to compare the differences in reactivity between mono- and multimetallic sites. Taking CO_2 photoreduction as the basic catalytic reaction, both compounds can achieve CO_2-to-$HCOO^-$ conversion with high selectivity (close to 100%). Moreover, the catalytic activity of multimetallic **Ti_{16}-C4A** is up to 2265.5 μmol g^{-1} h^{-1}, which is at least 12 times higher than that of monometallic **Ti-C4A** (180.0 μmol g^{-1} h^{-1}), and is the best-performing crystalline cluster-based photocatalyst known to date. Catalytic characterization combined with density functional theory calculations shows that in addition to the advantage of having more metal active sites (for adsorption and activation of more CO_2 molecules), **Ti_{16}-C4A** can effectively reduce the activation energy required for the CO_2 reduction reaction by completing the multiple electron−proton transfer process rapidly with synergistic metal−ligand catalysis, thus exhibiting superior catalytic performance to that of monometallic **Ti-C4A**. This work provides a crystalline catalyst model system to explore the potential factors underlying the difference in catalytic reactivity between mono- and multimetallic sites.

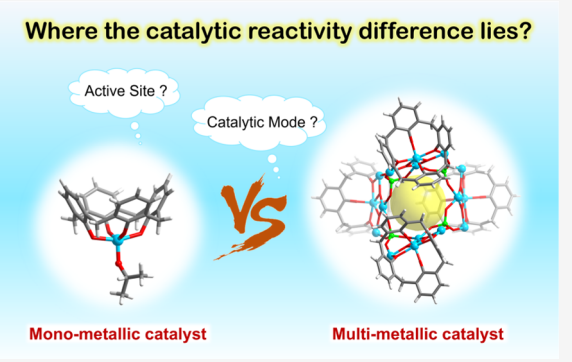

INTRODUCTION

In the past few decades, titanium dioxide (TiO_2) has evolved as a star photocatalyst for many photocatalytic applications owing to its inherent semiconductor characteristic and unique advantages, such as low cost, easy preparation, and nontoxicity.[1−4] But at the same time, the structural changes of crystal TiO_2 (single phase) generally only appear in three allotropes (rutile, anatase, and brookite),[5] leading to many limitations for their structural regulation and application of some specific photocatalytic reactions. Beyond that, the intrinsic ultraviolet photosensitivity of TiO_2 also seriously weakens the utilization efficiency of sunlight in photocatalytic reactions. Recently, titanium-oxo compounds (TOCs) with similar compositions to TiO_2 have developed rapidly.[6−13] Compared with TiO_2, TOCs have more diverse structures, and their intrinsic properties, such as stability, semiconductor-like behaviors, energy levels, and light absorption capacity, can be effectively regulated through modification with different functionalized organic ligands.[11,14−18] In particular, as an aggregate containing multiple metal ions, TOCs can create multiple active metal sites via rationally regulating the coordination environment of metal ions,[19−22] thus providing more opportunities for the catalytic activity improvement and application of photocatalytic reactions.

Photocatalytic reduction of CO_2 into reusable chemicals represents one of the most promising technologies to achieve carbon neutrality.[23−30] As one of the pioneer photocatalysts, TiO_2 was first discovered to achieve heterogeneous reduction of CO_2 into organic compounds such as formic acid, methane, formaldehyde, and methyl alcohol in water in 1979 but had relatively low yield and selectivity.[3] Since then, a lot of research studies have been devoted to regulate the structures, compositions, energy levels, and light absorption capacity of TiO_2 to improve its photocatalytic performance.[31−40] In this

Received: April 30, 2023

respect, TOCs obviously can easily achieve these regulations according to their unique advantages.[41−43] Nevertheless, currently reported TOCs capable of performing photocatalytic CO_2 reduction reactions (CO_2RRs) are still very limited. Particularly, TOCs that can perform the heterogeneous photocatalytic CO_2RR in water are extremely rare, mainly because most TOCs are soluble or lack sufficient strong bonding interactions to maintain their structural stability in water. To date, to the best of our knowledge, only our recently reported two calix[8]arene (C8A)-modified low-nuclearity TOCs (**Ti_4-C8A** and **Ti_7-C8A**) have been competent for heterogeneous photocatalytic CO_2RR in water.[21] These two TOCs maintain high stability in water and under photocatalytic reaction conditions, since the C8A molecule contains multiple hydrophobic phenyl groups and phenolate chelated sites. However, the high molecular freedom and multidirectional chelating modes of the C8A molecule make these two TOCs have less available metal active sites, leading to low photocatalytic performance.

Herein, we utilized calix[4]arene (C4A) as a functional ligand, which also contains multiple hydrophobic phenyl groups and phenolate chelated sites but has less molecular freedom, to construct three stable TOCs, $[Ti(C4A)(O^iPr)]\cdot$HTETN (**Ti-C4A**, HO^iPr = isopropanol, TETN = triethylamine), $[Ti_4O_2(C4A)_2(O^iPr)_4(DMF)_2]$ (**Ti_4-C4A**, DMF = *N*,*N*-dimethylformamide), and $[Ti_{16}O_8(C4A)_4(PO_4)_4(O^iPr)_{20}(HO^iPr)(H_2O)]\cdot H_2O$ (**Ti_{16}-C4A**), with increasing nuclearity and tunable light-harvesting ability (Scheme 1). Taking photocatalytic CO_2RR as the basic

Scheme 1. Illustration of the Structures of H_4C4A Ligand-Modified Mononuclear (Ti-C4A), Tetranuclear (Ti_4-C4A), and 16-Nuclear (Ti_{16}-C4A) TOCs

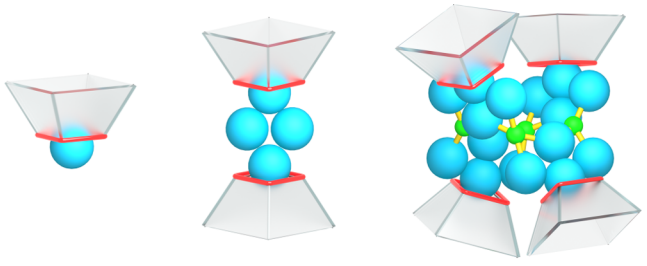

catalytic reaction, **Ti-C4A** and **Ti_{16}-C4A** demonstrated appropriate energy levels for the requirement of thermodynamic electrode potential of photoreducing CO_2 to the HCOOH product, in which **Ti_{16}-C4A** possesses more available metal active sites. The photocatalytic characterization results reveal that both **Ti-C4A** and **Ti_{16}-C4A** exhibit high catalytic activity (145.2−2265.5 μmol g^{-1} h^{-1}) and selectivity (close to 100%) of CO_2-to-$HCOO^-$ conversion under ultraviolet and visible light irradiation. Compared with monometallic active **Ti-C4A**, multimetallic active **Ti_{16}-C4A** achieved superior photocatalytic performance. In detail, the photocatalytic activity of **Ti_{16}-C4A** reaches 2265.5 μmol g^{-1} h^{-1}, which is about 12.6 times higher than that of **Ti-C4A** (180.0 μmol g^{-1} h^{-1}) and 8.9 and 4.6 times higher than those of our previously reported **Ti_4-C8A** (253.9 μmol g^{-1} h^{-1}) and **Ti_7-C8A** (488.4 μmol g^{-1} h^{-1}), respectively, under analogous photocatalytic conditions.[21] Notably, **Ti_{16}-C4A** with multimetallic active sites represents the best catalyst for photocatalytic CO_2-to-$HCOO^-$ reduction among crystalline cluster-based photocatalysts. Density functional theory (DFT) calculation results reveal that multimetallic **Ti_{16}-C4A** can not only adsorb and activate more CO_2 molecules than monometallic **Ti-C4A** but also use a synergistic metal−ligand catalytic effect to transfer electrons and protons more rapidly and then to lower the reaction activation energy, thus completing the CO_2 reduction process more effectively. More importantly, **Ti-C4A** and **Ti_{16}-C4A** in this work can constitute a crystalline model system to clearly indicate the reactivity advantages of multimetallic catalysts over monometallic catalysts and to explore the related underlying inducements.

RESULTS AND DISCUSSION

Brown-yellow crystals of **Ti-C4A** and **Ti_4-C4A** and yellow crystals of **Ti_{16}-C4A** were synthesized by the solvothermal reaction of titanium (IV) isopropoxide and the C4A ligand in different mixture solvents (Figure S1). Single-crystal X-ray diffraction analysis reveals that **Ti-C4A**, **Ti_4-C4A**, and **Ti_{16}-C4A** are mononuclear, tetranuclear, and 16-nuclear TOCs, respectively. **Ti-C4A** crystallizes in the orthorhombic space group $P2_12_12_1$ with one Ti atom, one $C4A^{4-}$ ligand, one isopropoxy anion ($-O^iPr$), and one triethylamine countercation in the asymmetric unit (Figure S2 and Tables S1 and S2). The Ti atom adopts a distorted tetragonal pyramid geometry with its equatorial sites occupied by four chelated phenolate O atoms from the $C4A^{4-}$ ligand and its axial site occupied by an $-O^iPr$ O atom (Figure 1b). In **Ti-C4A**, the Ti atom may serve as an active metal site, since the axial $-O^iPr$ anion may be substituted by another anionic species (such as OH^-) or first protonated and then substituted.

Ti_4-C4A crystallizes in the orthorhombic space group *Pbca* and its asymmetric unit contains two crystallographically independent Ti atoms (Ti1 and Ti2), one $C4A^{4-}$ ligand, two $-O^iPr$ anions, one μ_3-O atoms, and one coordinated DMF molecule (Figure S3). Both Ti1 and Ti2 atoms adopt distorted octahedral coordination geometry. As shown in Figure 1c, each Ti1 atom coordinates with four chelated phenolate O atoms, one μ_3-O atom, and one DMF molecule, while each Ti2 atom coordinates with two $-O^iPr$, two phenolate O atoms, and two μ_3-O atoms. Two Ti2 atoms are linked together by two μ_3-O atoms to form a binuclear unit, which is further connected with other two Ti1 atoms on two sides through μ_3-O and μ_2-O (from $C4A^{4-}$) atoms to form a robust tetranuclear Ti-oxo core with a planar diamond structure (Figure S3). The outer coordination space of this Ti-oxo core is surrounded by two $C4A^{4-}$ ligands, four $-O^iPr$, and two DMF.

Considering that a C4A ligand with a large molecular size may restrict the growth of the Ti-oxo core, we utilized a small chelated PO_4^{3-} anion as a second ligand to explore larger TOCs. Interestingly, a 16-nuclear TOC (**Ti_{16}-C4A**) was obtained (Figure 1d), which represents the largest calixarene-based TOC reported by far.[44−49]

Ti_{16}-C4A crystallizes in the triclinic space group $P\bar{1}$ and its asymmetric unit contains an intact molecule, which can be considered a tetrahedron with two edges missing. In this tetrahedron, its four vertices are occupied by four tetranuclear TOCs and four of the six edges are occupied by four PO_4^{3-} anions. The four tetranuclear TOCs (denoted Ti_4-C4A−A/B/C/D) have similar structures (Figure 2) but show slightly different coordination environments of the Ti atoms. In each tetranuclear TOC, there are four crystallographically independent Ti atoms (Ti1, Ti2, Ti3, and Ti4). As shown in Figure

https://doi.org/10.1021/jacs.3c04480
J. Am. Chem. Soc. XXXX, XXX, XXX−XXX

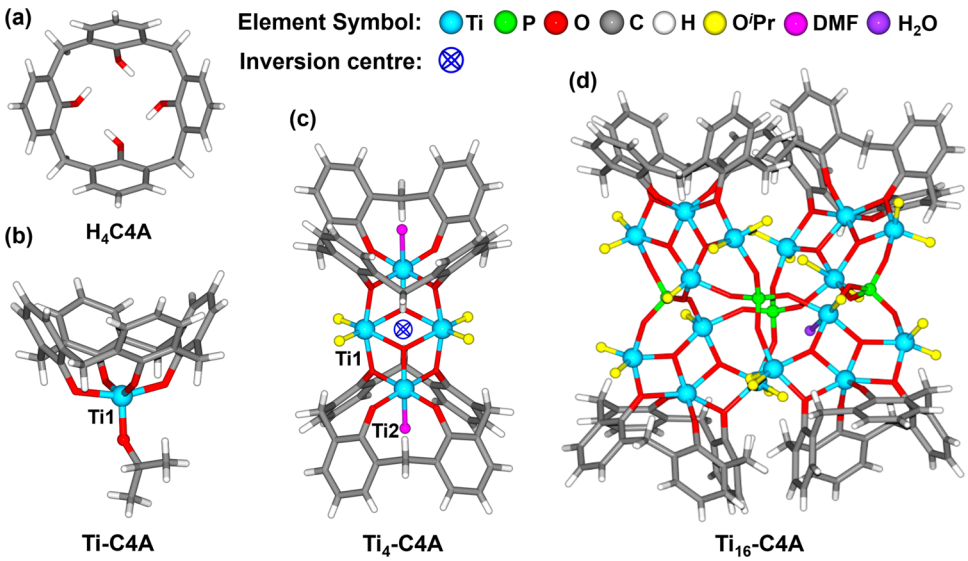

Figure 1. Molecular structures of (a) calix[4]arene (C4A), (b) mononuclear **Ti-C4A**, (c) tetranuclear **Ti_4-C4A**, and (d) 16-nuclear **Ti_{16}-C4A**. Color codes: sky blue = Ti atom, bright green = P atom, red = O atom, dark gray = C atom, gray-white = H atom, pink = O^{i}Pr ligand, yellow = DMF molecule, and violet = H_2O molecule.

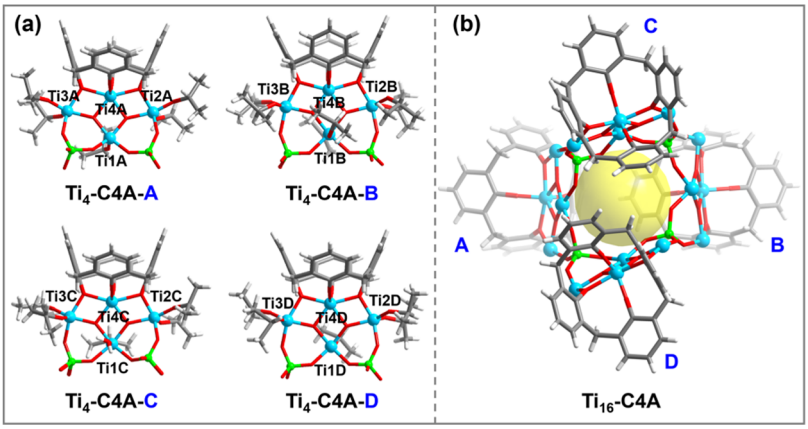

Figure 2. (a) Top view of the coordinated environment of the four tetranuclear TOCs (denoted Ti_4-C4A−A/B/C/D) in **Ti_{16}-C4A**. (b) The structure of **Ti_{16}-C4A** without coordinated solvent molecules.

2a, in Ti_4-C4A−A, the Ti1A atom coordinates with two PO_4^{3-} anions, two μ_3-O atoms, and one −O^{i}Pr ligand, featuring a distorted tetragonal pyramid coordination geometry. Similarly, Ti2A and Ti3A adopt distorted tetragonal pyramid geometry, while each Ti coordinates with one phenolate O atom, two μ_3-O atoms, and two −O^{i}Pr. Different from the other three Ti atoms, the Ti4A atom adopts distorted octahedral coordination geometry with its two equatorial sites and two axial sites occupied by four chelated phenolate O atoms and its other two equatorial sites filled by two μ_3-O atoms. These four Ti atoms are linked together by two phenolate μ_2-O atoms and two μ_3-O atoms to form a tetranuclear Ti-oxo core with a planar rhombic structure, which is different from that of **Ti_4-C4A**. Ti_4-C4A−B, Ti_4-C4A−C, and Ti_4-C4A−D have structures similar to Ti_4-C4A−A, except that Ti1B in Ti_4-C4A−B and the Ti1C atoms in Ti_4-C4A−C adopt octahedral coordination geometry (the axial sites are coordinated by two −O^{i}Pr for the Ti1B atom and one −O^{i}Pr and one H_2O molecule for the Ti1C atom; Figure 2a). These four tetranuclear TOCs are linked together by four PO_4^{3-} anions to form a 16-nuclear TOC with a robust tetrahedral configuration (Figure S4). It is worth noting that 12 Ti atoms in **Ti_{16}-C4A** are coordinated by −O^{i}Pr and H_2O, indicating that there are many potential active metal sites in this TOC (Figure 2b).

The crystals of **Ti-C4A**, **Ti_4-C4A**, and **Ti_{16}-C4A** exhibit yellow or brown-yellow color (Figure S1), and their solid-state UV−visible absorption spectra show significant absorption bands around 400, 500, and 450 nm (Figure 3a), respectively, suggesting they have better light absorption than TiO_2 (colorless TiO_2 or TOCs with absorption bands generally below 400 nm). Moreover, the adsorption bands of **Ti-C4A**, **Ti_4-C4A**, and **Ti_{16}-C4A** can be extended to 500, 800, and 600 nm, respectively. The good UV−visible light absorption of these TOCs should be attributed to the good electron-donating ability of C4A ligands and the high valance state of Ti^{4+} ions, which can make effective charge transfer from C4A ligands to Ti^{4+} ions.

Based on the UV−visible absorption spectra, the optical band gaps (E_g) of **Ti-C4A**, **Ti_4-C4A**, and **Ti_{16}-C4A** were calculated from the Tauc plots to be 1.90, 1.30, and 1.69 eV (Figure 3b), respectively, indicating that they possess semiconductor-like characteristics. To confirm this and determine

https://doi.org/10.1021/jacs.3c04480
J. Am. Chem. Soc. XXXX, XXX, XXX−XXX

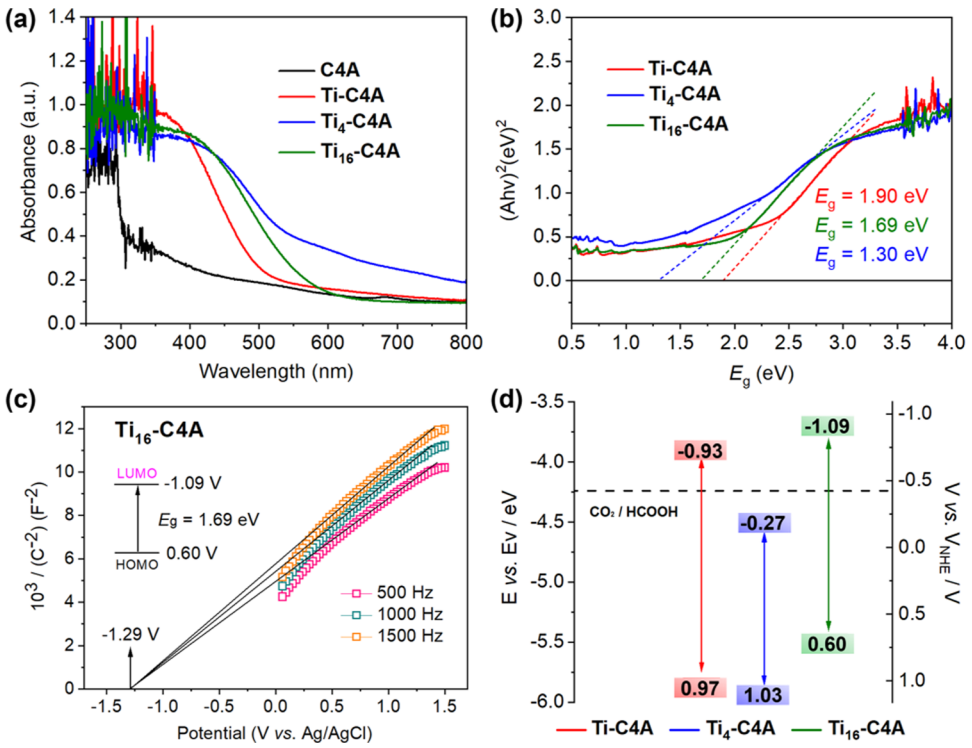

Figure 3. Solid-state UV−vis diffuse reflection spectra of the C4A ligand, **Ti-C4A**, **Ti_4-C4A**, and **Ti_{16}-C4A**. (b) Tauc plots of **Ti-C4A**, **Ti_4-C4A**, and **Ti_{16}-C4A**. (c) Mott−Schottky plot for **Ti_{16}-C4A** in a 0.2 M Na_2SO4 aqueous solution. The inset is the energy diagram of the HOMO and LUMO levels of **Ti_{16}-C4A**. (d) Energy band gap diagrams of **Ti-C4A**, **Ti_4-C4A**, and **Ti_{16}-C4A** with respect to the CO_2-to-HCOOH conversion.

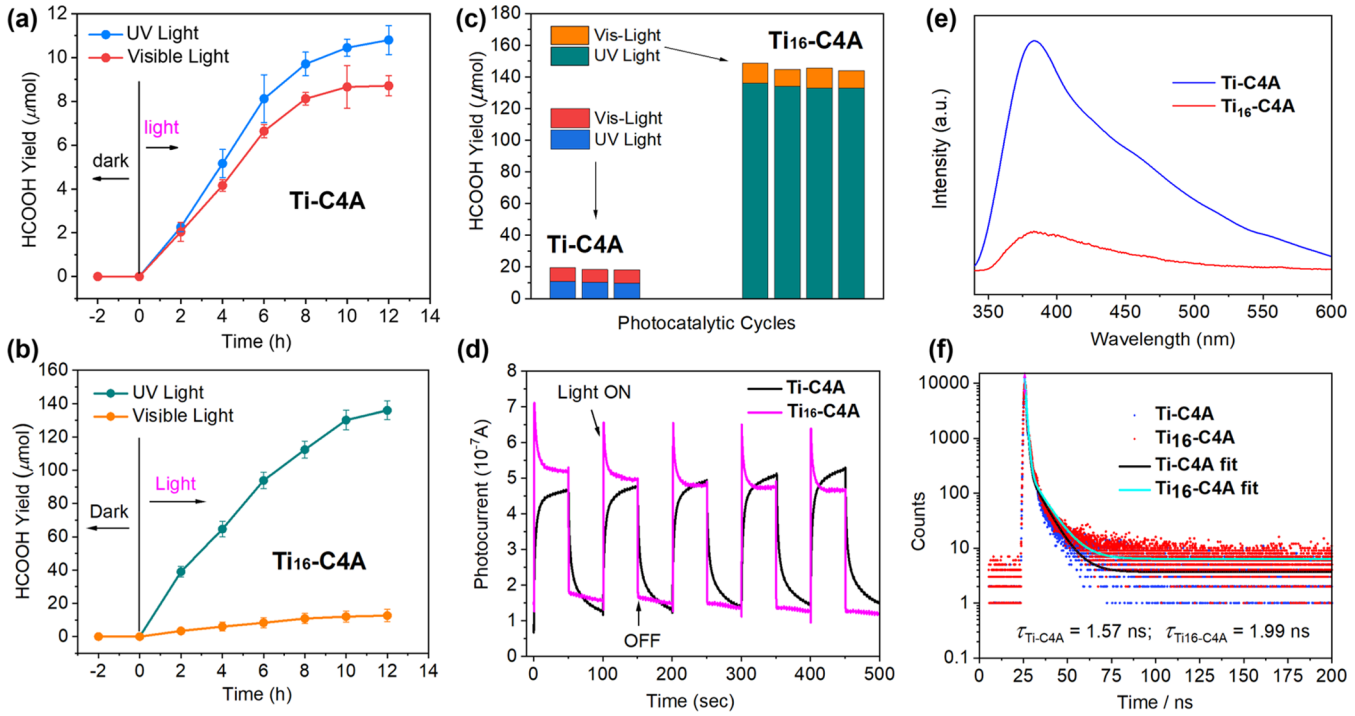

Figure 4. Relationship between the yield of $HCOO^-$ and the irradiation time (visible light) on (a) **Ti-C4A** and (b) **Ti_{16}-C4A**. (c) Yields of $HCOO^-$ for **Ti-C4A** and **Ti_{16}-C4A** photocatalysts in three continuous runs under visible or UV light irradiation. (d) Transient photocurrent responses of **Ti-C4A** and **Ti_{16}-C4A**. Xenon light as the light source was applied for photocurrent measurement, and a 0.1 M Tris-HCl aqueous solution was used as the electrolyte. (e) Steady-state photoluminescence (PL) spectra and (f) time-resolved emission decay profiles of **Ti-C4A** and **Ti_{16}-C4A**.

their flat-band potentials, Mott−Schottky measurements at frequencies of 500, 1000, and 1500 Hz were performed. As shown in Figures 3c, S6, and S7, the Mott−Schottky plots of **Ti-C4A**, **Ti_4-C4A**, and **Ti_{16}-C4A** exhibit positive slopes, confirming their n-type semiconductor-like characteristics. The flat-band potentials of **Ti-C4A**, **Ti_4-C4A**, and **Ti_{16}-C4A**

https://doi.org/10.1021/jacs.3c04480
J. Am. Chem. Soc. XXXX, XXX, XXX−XXX

were determined from the intersection to be −0.93, −0.27, and −1.09 V versus Ag/AgCl, respectively. Because the lowest unoccupied molecular orbital (LUMO) position in an n-type semiconductor is generally considered to be approximately equal to the flat-band potential, the LUMO positions of **Ti-C4A**, **Ti_4-C4A**, and **Ti_{16}-C4A** were calculated to be −0.93, −0.27, and −1.09 V (vs normal hydrogen electrode (NHE)), respectively (Figure 3d). Combined with the band gaps and LUMOs, the highest occupied molecular orbital (HOMO) positions of **Ti-C4A**, **Ti_4-C4A**, and **Ti_{16}-C4A** were evaluated to be 0.97, 1.03, and 0.60 V (vs NHE), respectively. Therefore, it is clear that except for **Ti_4-C4A**, the LUMO positions of **Ti-C4A** and **Ti_{16}-C4A** are more negative than the potential requirements of reducing CO_2 to many carbon-based products (such as HCOOH; Figure 3d), suggesting that they can serve as potential photocatalysts for CO_2RR.

Given the above advantages of these C4A-modified TOCs, we further investigate their photocatalytic activity for CO_2RR under UV and visible light irradiation. The photocatalytic reaction was carried out at 1 atm CO_2 in water with triethanolamine (TEOA) as the sacrificial electron donor (H_2O/TEOA = 4:1, 30 mL) and without addition of external photosensitizers. The reductive gas and liquid products were detected by gas chromatography (GC) and ion chromatography (IC), respectively. The results revealed that almost no CO_2 reduction products can be detected in both liquid and gas phases for **Ti_4-C4A** as a photocatalyst under UV or visible light irradiation, probably because the LUMO position of **Ti_4-C4A** (−0.27 V vs NHE) is lower than the CO_2 reduction potentials of most carbon-based products. In contrast, when **Ti-C4A** or **Ti_{16}-C4A** was used as a photocatalyst, an obvious $HCOO^-$ product could be detected in the liquid phase (Figure S8). As shown in Figure 4a,b, the $HCOO^-$ production increased continuously with the increase of UV or visible light irradiation time. Impressively, after UV light irradiation for 12 h, the $HCOO^-$ yield of **Ti_{16}-C4A** reached 136.0 μmol (2265.5 μmol g^{-1} h^{-1}), which is significantly higher than those of **Ti-C4A** (10.8 μmol after 12 h, 180.0 μmol g^{-1} h^{-1}) and our previously reported **Ti_4-C8A** and **Ti_7-C8A** (253.9 and 488.4 μmol g^{-1} h^{-1}, respectively), representing the highest value for $HCOO^-$ generation among crystal cluster-based photocatalysts under the similar reaction conditions.[21,50] The outstanding photocatalytic activity of **Ti_{16}-C4A** is probably related to its multiple (close to 12) potential Ti^{4+} catalytic active sites, including those coordinated with $-O^iPr/H_2O$ and naked coordination space (five-coordinated Ti atoms), which are available sites for the CO_2 attack. In contrast, there is only one potential Ti^{4+} catalytic active site in **Ti-C4A**, which results in relatively lower photocatalytic activity than that of **Ti_{16}-C4A**. Additionally, when an identical photocatalytic reaction was carried out under visible light irradiation (420−800 nm), the $HCOO^-$ yield (12.7 μmol; 211.0 μmol g^{-1} h^{-1}) of **Ti_{16}-C4A** is still slightly higher than that of **Ti-C4A** (8.7 μmol; 145.2 μmol g^{-1} h^{-1}), although both compounds exhibit weak visible light-harvesting capacities (Figure 4a,b). These results suggest that the multiple potential Ti^{4+} catalytic active sites in **Ti_{16}-C4A** are crucial for its outstanding photocatalytic performance. Importantly, except for $HCOO^-$, there are no other CO_2 reductive byproducts such as CO, CH_3OH, and CH_4 that can be detected in both liquid and gas phases during the UV and visible light-driven CO_2RR (Figure S9), suggesting high selectivity (~100%) toward the $HCOO^-$ product for **Ti-C4A** and **Ti_{16}-C4A** photocatalysts.

To evaluate the catalytic activity of each potential Ti^{4+} catalytic active site in **Ti-C4A** and **Ti_{16}-C4A**, we calculated their turnover number (TON_{Ti}) by assuming that there are 1 and 12 potential Ti active centers in each **Ti-C4A** and **Ti_{16}-C4A** molecules, respectively, based on their crystal structures. As shown in Table S3, under UV light irradiation, the TON_{Ti} of **Ti_{16}-C4A** is 9.6, which is about 7-fold that of **Ti-C4A** (1.4) under the same reaction condition, indicating that the Ti^{4+} catalytic sites in **Ti_{16}-C4A** are much more active than those in **Ti-C4A** for UV light-driven CO_2 reduction into $HCOO^-$. To further explore the reasons behind the different photocatalytic activities between **Ti-C4A** and **Ti_{16}-C4A**, the photocurrent response test was conducted under UV−vis light irradiation to evaluate the photoinduced electron transfer efficiency. Interestingly, both **Ti-C4A** and **Ti_{16}-C4A** exhibit similar strong photocurrent responses, implying that the photoinduced electron−hole separation efficiencies are similar for these two compounds. To confirm this, the photoluminescence (PL) spectra and PL decay lifetimes of these two compounds were tested. As shown in Figure 4e,f, although the PL intensity of **Ti_{16}-C4A** is lower than that of **Ti-C4A**, the PL decay lifetimes of these two compounds are quite similar ($\tau_{Ti\text{-}C4A}$ = 1.57 ns, $\tau_{Ti16\text{-}C4A}$ = 1.99 ns), suggesting that **Ti-C4A** and **Ti_{16}-C4A** indeed have similar electron−hole pair separation efficiency.[51] Therefore, the outstanding performance of **Ti_{16}-C4A** in the photocatalytic CO_2 reduction to $HCOO^-$ may be attributed to the multiple Ti^{4+} catalytic active sites and the possible synergistic metal−ligand catalysis effect.

Because the crystals of **Ti-C4A** and **Ti_{16}-C4A** did not dissolve and showed good crystallinities after the photocatalytic CO_2RR, they should belong to heterogeneous catalysts. To confirm this, the solid catalysts were separated after the photocatalytic CO_2RR and the filtrates were determined by an inductively coupled plasma mass spectrometer (ICP-MS) and UV−vis absorption spectra. The results revealed that the Ti^{4+} ions in the filtrates are only about 0.034 and 0.051% for **Ti-C4A** and **Ti_{16}-C4A**, respectively. Besides, there are no obvious new signals of the UV−visible absorption spectra of the filtrates, excluding the dissolution of **Ti-C4A** and **Ti_{16}-C4A** during the photocatalytic CO_2RR (Figure S10). In addition, the solid infrared (IR) spectra and powder X-ray diffraction (PXRD) patterns of **Ti-C4A** and **Ti_{16}-C4A** before and after photocatalytic CO_2RR are nearly unchanged (Figures S11−S14), confirming their high crystallinity and heterogeneous catalytic nature. To further demonstrate the heterogeneous catalytic nature and catalytic stability of **Ti-C4A** and **Ti_{16}-C4A** in water, recycling photocatalytic tests under both UV and visible light irradiation were conducted. After 12 h of photocatalysis, the catalyst was isolated by filtration, washed with water, dried under vacuum, and then used for further photocatalysis. The results revealed that **Ti-C4A** and **Ti_{16}-C4A** can maintain their activities for at least 36 h (three cycles; Figure 4c). The slightly decreased $HCOO^-$ yield was probably because of the inevitable loss of the catalyst during recycling and reactivation. Therefore, these recycling and long-term experiments demonstrated that **Ti-C4A** and **Ti_{16}-C4A** belonged to heterogeneous catalysts and have stable catalytic activity in water. It is worth noting that most reported cluster-based molecular catalysts are homogeneous catalysts and generally perform photocatalytic CO_2RR in organic solvents (most are in pure organic solvents, such as acetonitrile). Besides, in addition to sacrificial agents, they usually need precious metal photosensitizers to improve their light-harvest-

https://doi.org/10.1021/jacs.3c04480
J. Am. Chem. Soc. XXXX, XXX, XXX−XXX

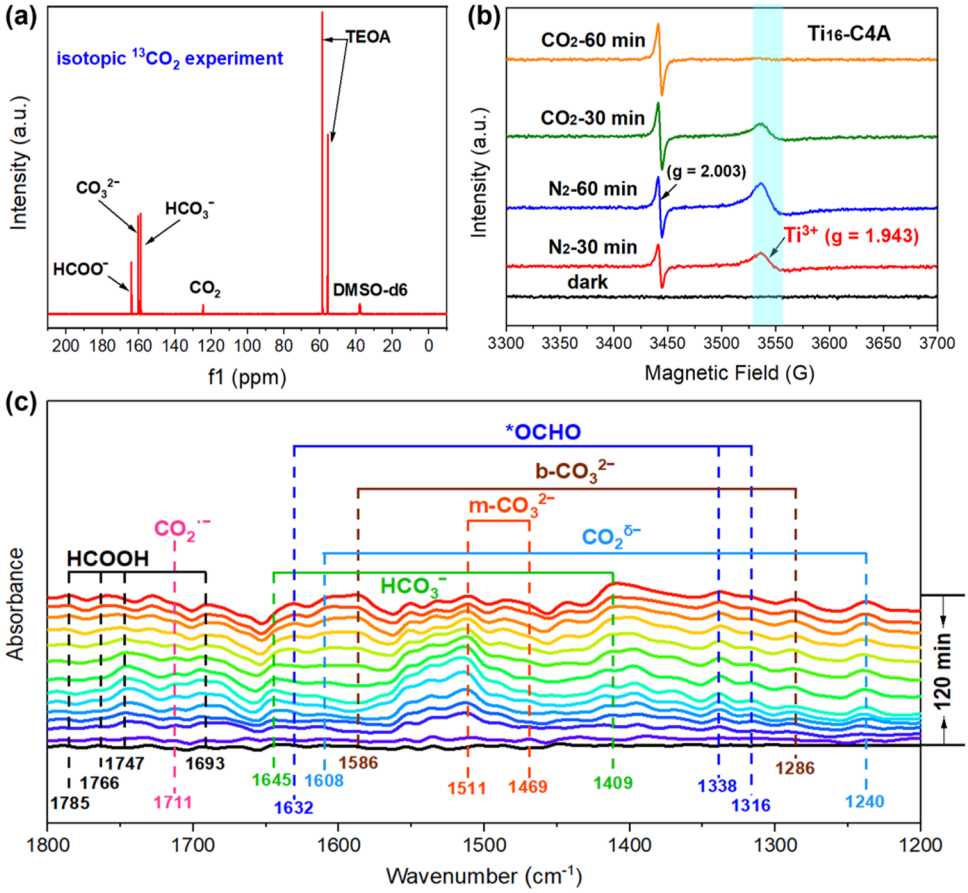

Figure 5. (a) ^{13}C NMR spectrum of the reaction solution catalyzed with the **Ti_{16}-C4A** photocatalyst under a $^{13}CO_2$ atmosphere. (b) EPR spectra of **Ti_{16}-C4A** under UV light irradiation and a CO_2 or N_2 atmosphere. (c) In situ FTIR spectra on **Ti_{16}-C4A** under UV light irradiation and a CO_2 atmosphere.

ing capacities for effective photocatalytic performance. In contrast, these two C4A ligand-modified **Ti-C4A** and **Ti_{16}-C4A** TOCs can act as heterogeneous catalysts and exhibit high catalytic activity and selectivity of photocatalytic CO_2 reduction to $HCOO^-$ in H_2O, without the need for precious photosensitizers, which is important in the terms of cost and environment friendliness.

To further demonstrate the photocatalytic CO_2 reduction activities of **Ti-C4A** and **Ti_{16}-C4A**, a series of control experiments were carried out, including reactions in the absence of light, catalyst, CO_2, or TEOA (Table S4). The results reveal that no CO_2 reductive products can be detected through IC and GC during (online detection) or after the reaction (liquid product identification) in these conditions, implying that **Ti-C4A** and **Ti_{16}-C4A** are indeed capable of photocatalytic reduction of CO_2 to $HCOO^-$. To further confirm this, carbon-13 labeling experiments using $^{13}CO_2$ were carried out with more active **Ti_{16}-C4A** as a heterogeneous photocatalyst under identical reaction conditions (UV light irradiation), and the products were identified by ^{13}C NMR spectroscopy. As shown in Figure 5a, the ^{13}C NMR spectrum exhibits obvious signals at 158.9, 160.2, and 163.9 ppm, which correspond to HCO_3^-, CO_3^{2-}, and $HCOO^-$, respectively.[52] Impressively, owing to the outstanding photocatalytic performance of **Ti_{16}-C4A**, the $HCOO^-$ signal in ^{13}C NMR spectroscopy is very strong, which is rarely observed for photocatalytic CO_2RR. In contrast, when an identical reaction was carried out under $^{12}CO_2$, no $HCO\bar{O}$ signal could be detected by ^{13}C NMR spectroscopy (Figure S15), demonstrating that the carbon source of the produced $HCOO^-$ originated from CO_2, and **Ti_{16}-C4A** is indeed active for reducing CO_2 to $HCOO^-$ under UV light irradiation.

Encouraged by the outstanding performance of **Ti_{16}-C4A** in the photocatalytic CO_2 reduction to $HCOO^-$, the mechanism of photocatalyzed CO_2RR was studied based on this catalyst by using electron paramagnetic resonance (EPR) spectroscopy. As shown in Figure 5b, **Ti_{16}-C4A** did not show ERP signals without light irradiation under a N_2 atmosphere. In contrast, sharp signals that correspond to Ti^{3+} species (g = 1.943) emerged upon light irradiation under a N_2 atmosphere.[50] This is because the Ti-oxo core of **Ti_{16}-C4A** accepts electrons from the linkers through ligand-to-cluster charge transfer (LCCT) after photoexcitation, and Ti^{4+} in the Ti-oxo core was reduced to form Ti^{3+}, while under continuous light irradiation in a CO_2 atmosphere for 1 h, the ERP signal of Ti^{3+} decreased significantly, indicating that the Ti^{3+} species was involved in the photo-driven CO_2RR.[50,53] Thus, the photoexcitation can be rationalized as follows: upon light irradiation, e^- migrate from the photoexcited linker to the Ti-oxo cluster for reducing Ti^{4+} to Ti^{3+} species, while TEOA acts as an h^+ scavenger. Then, e^- are transferred from the Ti^{3+} species to CO_2 adsorbed on the active metal site, accompanied by the conversion of Ti^{3+} to Ti^{4+} species. Therefore, the photocatalytic cycle of CO_2-to-$HCOO^-$ conversion is achieved in the presence of TEOA as the electron donor. In this process, TEOA might be oxidized to its aldehyde form (Figure S16).

https://doi.org/10.1021/jacs.3c04480
J. Am. Chem. Soc. XXXX, XXX, XXX−XXX

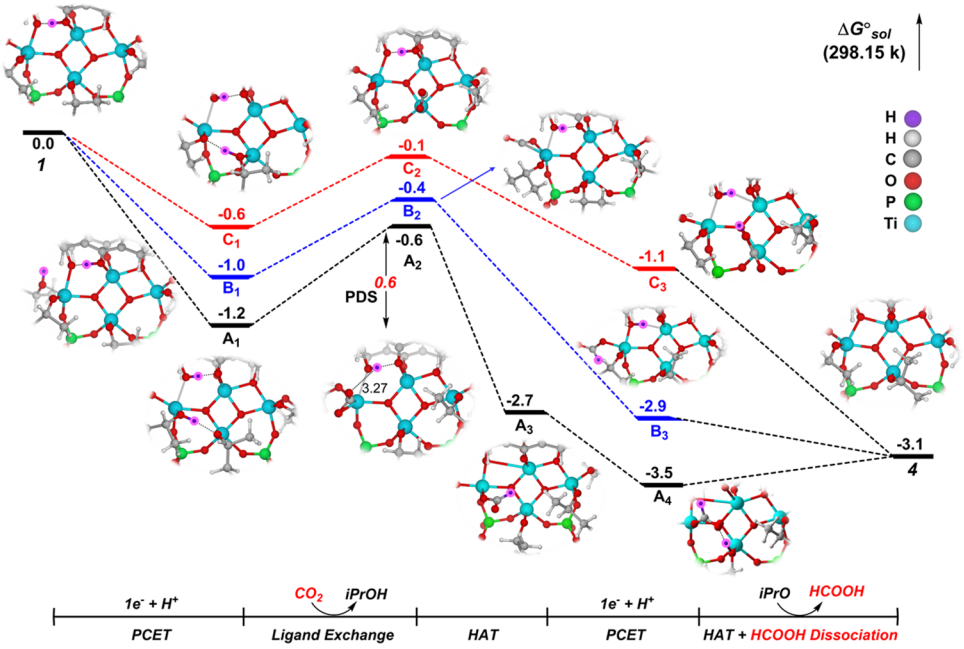

Figure 6. Mechanism and potential energy surfaces of the **Ti_{16}-C4A** catalytic process. The CO_2-to-HCOOH conversion reactive pathways over the tetranuclear Ti-oxo unit of **Ti_{16}-C4A**, and the corresponding Gibbs energy and intermediate architectures.

To investigate the reasons for the high selectivity of the catalyst to $HCOO^-$, in situ diffuse reflectance infrared Fourier transform spectroscopy (DRIFTS) was performed to detect CO_2 radicals and other reaction intermediates of the catalytic process. As shown in Figure 5c, no significant changes in the vibrational peaks were observed before illumination. With increasing lighting time, new peaks obviously appeared and their intensities gradually increased. The absorption peaks at 1316, 1338, 1469, and 1511 cm^{-1} are attributed to monodentate carbonate (m-CO_3^{2-}),[54] while those at 1286 and 1586 cm^{-1} can be attributed to bidentate carbonate (b-CO_3^{2-}).[55] A significant enhancement of the absorption peak could be observed at 1711 cm^{-1}, where the peak was attributed to $CO_2^{\bullet-}$, which is an important one-electron reductive intermediate in the photocatalytic reduction of CO_2 to $HCOO^-$.[22] The simultaneous appearance of absorption peaks at 1240 and 1608 cm^{-1} indicated the formation of carboxylate ($CO_2^{\delta-}$).[56] The absorption peaks located at 1693, 1747, 1766, and 1785 cm^{-1} were probably from formic acid.[57]

To gain more insights into the photocatalytic mechanism, DFT calculations related to CO_2 adsorption and activation were carried out for **Ti_{16}-C4A** and **Ti-C4A** (see the Supporting Information for details). Considering that **Ti_{16}-C4A** and **Ti-C4A** behave as heterogeneous catalysts, the reaction mechanism should be studied through the solid surface rather than individual molecules. However, the crystalline catalyst solid is essentially composed of identical molecules stacked periodically. In this case, it is generally assumed that the mechanism by which the catalytic reaction occurs on the solid surface or on individual molecule is similar. Therefore, the DFT calculation study focused on the molecular reaction mechanism. Owing to the large size of **Ti_{16}-C4A**, the simplified molecular model is beneficial for exploring the catalytic reaction process more conveniently. After the structural optimization, we found that the four tetranuclear units in **Ti_{16}-C4A** have quite similar structures. Besides, density of states calculations reveal that a unit cell of the catalyst **Ti_{16}-Cluster** molecule and a quarter of the **Ti_{16}-Cluster** molecule (i.e., Ti_4-cluster fragment) have similar electronic state density distributions and energy gaps (Figure S17), suggesting that it is feasible to utilize the tetranuclear unit (Ti_4-cluster fragment) as a model for investigating the photocatalytic mechanism of **Ti_{16}-C4A**. First, the adsorbed sites of the first electron and proton on the tetranuclear unit were investigated. The results reveal that the electron is delocalized on the four Ti metal centers, while the proton is more likely to interact with the phenolate O atom of C4A (denoted intermediate 1, Figures 6 and S18), rather than the coordinated $-O^iPr$ oxygen atoms (denoted intermediate 2 and 3, Figure S19). Using intermediate 1 as the started model, the second electron and proton were offered to create an activated Ti metal center (intermediates 2 and 3 as started models have also been investigated, Figures S20 and S21). As shown in Figures 6 and S18, the protons were added to three different $-O^iPr$ oxygen atoms, including two coordinated Ti atoms on the left side and one coordinated Ti atom on the bottom (Ti atom at the right side can be viewed as equal to that at the left side), resulting in three different intermediates with Gibbs free energies (ΔG) of −1.2 (for A_1), −1.0 (for B_1), and −0.6 eV (for C_1). In addition, the protons adsorbed on the phenolate O atom and the top Ti atom were also considered (Figure S22), but the results reveal that these two cases show higher ΔG (1.2 and 2.8 eV, compared with A_1), suggesting that they are unfavorable cases. With the adsorbing proton, the coordinated $-O^iPr$ group becomes a neutral molecule and thus can easily leave from the Ti atoms to build open active metal sites for adsorbing and converting the CO_2 molecule to COO^- species. The resulting intermediates A_2, B_2, and C_2 with adsorbing COO^- show higher ΔG, suggesting that this is an endothermic process. Interestingly, in the intermediates of A_2 and B_2, COO^- is more likely to coordinate with the Ti atom by both C and O atoms, while in C_2, COO^- is more likely to use the O atom to coordinate with the Ti atom. Besides, in A_2, the adsorbed $*COO^-$ is close to the proton adsorbed on the phenolate O

https://doi.org/10.1021/jacs.3c04480
J. Am. Chem. Soc. XXXX, XXX, XXX−XXX

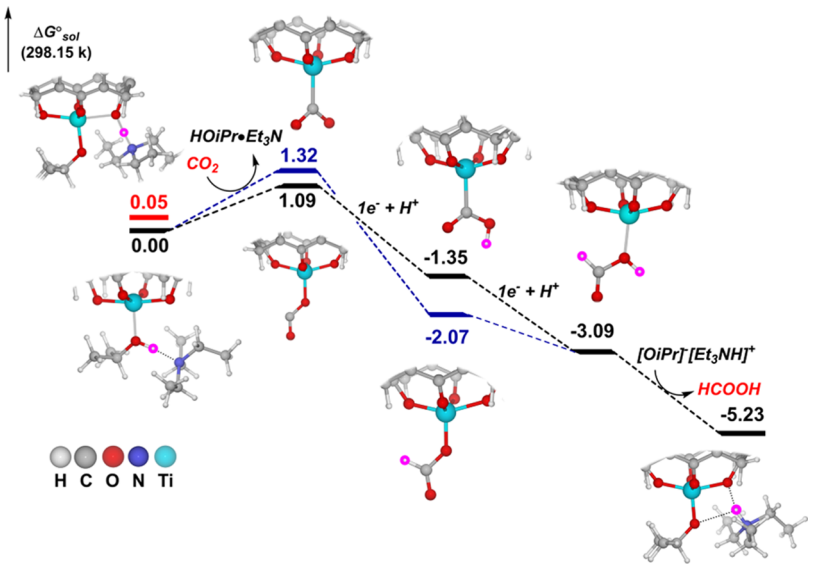

Figure 7. Mechanism and potential energy surfaces of the **Ti-C4A** catalytic process. The CO_2-to-HCOOH conversion reactive pathways over **Ti-C4A**, and the corresponding Gibbs energy and intermediate architectures.

atom. Thus, the proton is easy to transfer to the $*COO^-$ group to generate *OCHO (ΔG = −2.1 eV), which has also been observed in in situ DRIFTS spectroscopy (Figure 5c). Finally, HCOOH can be obtained through a proton-coupled electron transfer (PCET) process and a ligand exchange process with ΔG falling to −3.1 eV. The overall calculation results indicate that CO_2RR can readily occur at different potential Ti active sites through path A (black line), path B (blue line), or path C (red line). Nevertheless, compared with paths B and C, path A is considered to be more favorable, since all reaction intermediates are more stable in path A than in paths B and C. The adsorption of CO_2 is the potential determining step (ΔG = 0.6 eV for path A) for the elementary reaction steps. Additionally, the phenolate O atom can serve as a proton adsorption site, and the adsorbed proton can be subsequently transferred to the reaction intermediate $*COO^-$ that coordinated on the adjacent Ti active site, thus facilitating the CO_2RR. Therefore, the excellent photocatalytic performance of **Ti_{16}-C4A** should be mainly attributed to multiple Ti active sites and the synergistic catalytic effect between the Ti active site and the C4A ligand.

The photocatalytic CO_2RR mechanism of **Ti-C4A** was also investigated by DFT calculations (Figure S23). The results reveal that the first proton is more likely to interact with the coordinated $-O^iPr$ oxygen atom (Figures 7 and S24), rather than the phenolate O atom of the C4A ligand, which is different from the case in **Ti_{16}-C4A**. After adsorbing one proton, the Ti−O bond length was extended from 1.83 to 2.07 Å, and the H proton on the neighboring triethylamine countercation was detached, suggesting that the coordinated $-O^iPr$ group became a neutral molecule. On the other hand, the Ti^{4+} atom accepted the first electron and was reduced to Ti^{3+}, which thus can further absorb a CO_2 molecule through a ligand exchange process. The CO_2 adsorbed on the Ti atom intends to form an $*OCO^-$ intermediate rather than a $*COO^-$ intermediate ($\Delta G(*OCO^-)$ = 1.09 eV, $\Delta G(*COO^-)$ = 1.32 eV). DFT calculation revealed that the active Ti(IV) site preferred to interact with the p orbital of the O atom of CO_2 in **Ti-C4A**, resulting in the adsorption of the CO_2 molecule through the formation of a Ti−O bond (Figure S25a). In contrast, in **Ti_{16}-C4A**, the active Ti(IV) site is more inclined to interact with the π orbital of the C═O of CO_2, resulting in the adsorption of CO_2 molecules through the formation of a Ti−CO tri-atom-centered covalent bond (Figure S25b). Finally, HCOOH can be obtained through two PCET processes and a ligand exchange process. Similarly, the potential determining step for the photocatalytic CO_2RR in **Ti-C4A** is the adsorption of CO_2, but it exhibits a higher ΔG value (1.09 eV) than that observed in **Ti_{16}-C4A**. These calculation results suggest that CO_2RR can also occur at the Ti active site for **Ti-C4A**, but due to the lack of multiple active sites and the synergistic catalytic effect, it thus shows ordinary catalytic performance compared with **Ti_{16}-C4A**.

Additionally, considering that the photocatalytic CO_2RR was performed in water, the $-O^iPr$ groups on the catalysts may be replaced by OH^- groups, which were further protonated and then substituted by CO_2. Therefore, the catalytic mechanism in this case was also investigated. For **Ti_{16}-C4A**, two possibilities were considered. First, the $-O^iPr$ groups at the catalytic sites were replaced by OH^- groups, while those at the non-catalytic sites remained (Figure S26). Second, all $-O^iPr$ groups on the tetranuclear Ti-oxo unit were replaced by OH^- groups (Figure S27). The results revealed that there was no obvious difference in ΔG for the $-O^iPr$ coordinated intermediates and the OH^- coordinated intermediates. Moreover, after being replaced with OH^- groups, the adsorption of CO_2 is still the potential determining step (ΔG = 0.6−0.8 eV) for the elementary reaction steps. Similarly, for **Ti-C4A**, additional DFT calculations were performed by considering that the $-O^iPr$ group was replaced by the OH^- group. The results also revealed that there was no obvious difference in ΔG for the intermediates of these two calculation models (Figure S28).

CONCLUSIONS

In summary, we have successfully synthesized three stable C4A-functionalized TOCs with increasing nuclearity as well as tunable light absorption capacity and energy levels, among which **Ti-C4A** and **Ti_{16}-C4A** can serve as model catalysts for perceiving the difference in catalytic reactivity between mono-

https://doi.org/10.1021/jacs.3c04480
J. Am. Chem. Soc. XXXX, XXX, XXX−XXX

and multimetallic sites. By using CO_2 photoreduction as the basic reaction, both two compounds can be treated as heterogeneous photocatalysts to achieve high selectivity (ca. 100%) for CO_2-to-$HCOO^-$ conversion in water. Experimental characterization and DFT calculations indicated that **Ti_{16}-C4A** combines the advantages of multiple active metal sites and synergistic metal−ligand catalysis, which can effectively convert more CO_2 molecules while lowering the activation energy of the reaction, and thus exhibits superior photocatalytic activity (2265.5 μmol g^{-1} h^{-1}) than **Ti-C4A**. Moreover, **Ti_{16}-C4A** is also the best-performing crystalline cluster-based photocatalyst in photocatalytic CO_2RR. This work provides an important case study and demonstrates the great potential of crystalline model systems for exploring the structure−property relationship of catalysts.

■ ASSOCIATED CONTENT

Supporting Information

The Supporting Information is available free of charge at https://pubs.acs.org/doi/10.1021/jacs.3c04480.

Detailed information regarding the experimental methods; characterization analysis; DFT calculations; and CIF file (PDF)

Accession Codes

CCDC 2233755−2233757 contain the supplementary crystallographic data for this paper. These data can be obtained free of charge via www.ccdc.cam.ac.uk/data_request/cif, or by emailing data_request@ccdc.cam.ac.uk, or by contacting The Cambridge Crystallographic Data Centre, 12 Union Road, Cambridge CB2 1EZ, UK; fax: +44 1223 336033.

■ AUTHOR INFORMATION

Corresponding Authors

Jun He − *Department School of Chemical Engineering and Light Industry, Guangdong University of Technology, Guangzhou 510006 Guangdong, China;* orcid.org/0000-0001-7062-4001; Email: junhe@gdut.edu.cn

Ya-Qian Lan − *National and Local Joint Engineering Research Center of MPTES in High Energy and Safety LIBs, Engineering Research Center of MTEES (Ministry of Education), and Key Lab. of ETESPG (GHEI), School of Chemistry, South China Normal University, Guangzhou 510006, China;* orcid.org/0000-0002-2140-7980; Email: yqlan@m.scnu.edu.cn

Authors

Ning Li − *Department School of Chemical Engineering and Light Industry, Guangdong University of Technology, Guangzhou 510006 Guangdong, China*

Jiao-Min Lin − *National and Local Joint Engineering Research Center of MPTES in High Energy and Safety LIBs, Engineering Research Center of MTEES (Ministry of Education), and Key Lab. of ETESPG (GHEI), School of Chemistry, South China Normal University, Guangzhou 510006, China*

Run-Han Li − *National and Local Joint Engineering Research Center of MPTES in High Energy and Safety LIBs, Engineering Research Center of MTEES (Ministry of Education), and Key Lab. of ETESPG (GHEI), School of Chemistry, South China Normal University, Guangzhou 510006, China*

Jing-Wen Shi − *National and Local Joint Engineering Research Center of MPTES in High Energy and Safety LIBs, Engineering Research Center of MTEES (Ministry of Education), and Key Lab. of ETESPG (GHEI), School of Chemistry, South China Normal University, Guangzhou 510006, China*

Long-Zhang Dong − *National and Local Joint Engineering Research Center of MPTES in High Energy and Safety LIBs, Engineering Research Center of MTEES (Ministry of Education), and Key Lab. of ETESPG (GHEI), School of Chemistry, South China Normal University, Guangzhou 510006, China;* orcid.org/0000-0002-9276-5101

Jiang Liu − *National and Local Joint Engineering Research Center of MPTES in High Energy and Safety LIBs, Engineering Research Center of MTEES (Ministry of Education), and Key Lab. of ETESPG (GHEI), School of Chemistry, South China Normal University, Guangzhou 510006, China;* orcid.org/0000-0002-2596-4928

Complete contact information is available at: https://pubs.acs.org/10.1021/jacs.3c04480

Author Contributions

[§]N.L., J.-M.L., and R.-H.L. contributed equally to this work.

Notes

The authors declare no competing financial interest.

■ ACKNOWLEDGMENTS

This study was financially supported by the National Natural Science Foundation of China (Nos. 22201046, 21871061, and 21871141), the China Postdoctoral Science Foundation (Nos. 15 Special Fund (In-Station) 2022T150143 and 2021M700877), Guangdong Basic and Applied Basic Research Foundation (No. 2023A1515030097), and Local Innovative and Research Teams Project of Guangdong Pearl River Talents Program (2017BT01Z032).

■ REFERENCES

(1) Hoffmann, M. R.; Martin, S. T.; Choi, W.; Bahnemann, D. W. Environmental Applications of Semiconductor Photocatalysis. *Chem. Rev.* **1995**, *95*, 69−96.

(2) Schneider, J.; Matsuoka, M.; Takeuchi, M.; Zhang, J.; Horiuchi, Y.; Anpo, M.; Bahnemann, D. W. Understanding TiO2 Photocatalysis: Mechanisms and Materials. *Chem. Rev.* **2014**, *114*, 9919−9986.

(3) Inoue, T.; Fujishima, A.; Konishi, S.; Honda, K. Photoelectrocatalytic reduction of carbon dioxide in aqueous suspensions of semiconductor powders. *Nature* **1979**, *277*, 637−638.

(4) Dhakshinamoorthy, A.; Navalon, S.; Corma, A.; Garcia, H. Photocatalytic CO2 reduction by TiO2 and related titanium containing solids. *Energy Environ. Sci.* **2012**, *5*, 9217−9233.

(5) Chen, X.; Mao, S. S. Titanium Dioxide Nanomaterials: Synthesis, Properties, Modifications, and Applications. *Chem. Rev.* **2007**, *107*, 2891−2959.

(6) Coppens, P.; Chen, Y.; Trzop, E. Crystallography and Properties of Polyoxotitanate Nanoclusters. *Chem. Rev.* **2014**, *114*, 9645−9661.

(7) Rozes, L.; Sanchez, C. Titanium oxo-clusters: precursors for a Lego-like construction of nanostructured hybrid materials. *Chem. Soc. Rev.* **2011**, *40*, 1006−1030.

(8) Zhang, G.; Liu, C.; Long, D.-L.; Cronin, L.; Tung, C.-H.; Wang, Y. Water-Soluble Pentagonal-Prismatic Titanium-Oxo Clusters. *J. Am. Chem. Soc.* **2016**, *138*, 11097−11100.

(9) Zhang, L.; Fan, X.; Yi, X.; Lin, X.; Zhang, J. Coordination-Delayed-Hydrolysis Method for the Synthesis and Structural Modulation of Titanium-Oxo Clusters. *Acc. Chem. Res.* **2022**, *55*, 3150−3161.

https://doi.org/10.1021/jacs.3c04480
J. Am. Chem. Soc. XXXX, XXX, XXX−XXX

(10) Fang, W.-H.; Zhang, L.; Zhang, J. A 3.6 nm Ti_{52}−Oxo Nanocluster with Precise Atomic Structure. *J. Am. Chem. Soc.* **2016**, *138*, 7480−7483.
(11) Benedict, J. B.; Freindorf, R.; Trzop, E.; Cogswell, J.; Coppens, P. Large Polyoxotitanate Clusters: Well-Defined Models for Pure-Phase TiO2 Structures and Surfaces. *J. Am. Chem. Soc.* **2010**, *132*, 13669−13671.
(12) Sokolow, J. D.; Trzop, E.; Chen, Y.; Tang, J.; Allen, L. J.; Crabtree, R. H.; Benedict, J. B.; Coppens, P. Binding Modes of Carboxylate- and Acetylacetonate-Linked Chromophores to Homodisperse Polyoxotitanate Nanoclusters. *J. Am. Chem. Soc.* **2012**, *134*, 11695−11700.
(13) Zhang, G.; Li, W.; Liu, C.; Jia, J.; Tung, C.-H.; Wang, Y. Titanium-Oxide Host Clusters with Exchangeable Guests. *J. Am. Chem. Soc.* **2018**, *140*, 66−69.
(14) Fan, X.; Wang, J.; Wu, K.; Zhang, L.; Zhang, J. Isomerism in Titanium-Oxo Clusters: Molecular Anatase Model with Atomic Structure and Improved Photocatalytic Activity. *Angew. Chem., Int. Ed.* **2019**, *58*, 1320−1323.
(15) Padial, N. M.; Castells-Gil, J.; Almora-Barrios, N.; Romero-Angel, M.; da Silva, I.; Barawi, M.; García-Sánchez, A.; de la Peña O'Shea, V. A.; Martí-Gastaldo, C. Hydroxamate Titanium−Organic Frameworks and the Effect of Siderophore-Type Linkers over Their Photocatalytic Activity. *J. Am. Chem. Soc.* **2019**, *141*, 13124−13133.
(16) Wang, S.; Cabrero-Antonino, M.; Navalón, S.; Cao, C.-c.; Tissot, A.; Dovgaliuk, I.; Marrot, J.; Martineau-Corcos, C.; Yu, L.; Wang, H.; Shepard, W.; García, H.; Serre, C. A Robust Titanium Isophthalate Metal-Organic Framework for Visible-Light Photocatalytic CO2 Methanation. *Chem* **2020**, *6*, 3409−3427.
(17) Lv, S.-Y.; Liu, Q.-Y.; Zhao, Y.-X.; He, S.-G. Photooxidation of Isoprene by Titanium Oxide Cluster Anions with Dimensions up to a Nanosize. *J. Am. Chem. Soc.* **2021**, *143*, 3951−3958.
(18) Padial, N. M.; Lerma-Berlanga, B.; Almora-Barrios, N.; Castells-Gil, J.; da Silva, I.; de la Mata, M.; Molina, S. I.; Hernández-Saz, J.; Platero-Prats, A. E.; Tatay, S.; Martí-Gastaldo, C. Heterometallic Titanium−Organic Frameworks by Metal-Induced Dynamic Topological Transformations. *J. Am. Chem. Soc.* **2020**, *142*, 6638−6648.
(19) Su, K.; Wu, M.; Tan, Y.; Wang, W.; Yuan, D.; Hong, M. A monomeric bowl-like pyrogallol[4]arene Ti_{12} coordination complex. *Chem. Commun.* **2017**, *53*, 9598−9601.
(20) Liu, J.-J.; Sun, S.-N.; Liu, J.; Kuang, Y.; Shi, J.-W.; Dong, L.-Z.; Li, N.; Lu, J.-N.; Lin, J.-M.; Li, S.-L.; Lan, Y.-Q. Achieving High-Efficient Photoelectrocatalytic Degradation of 4-Chlorophenol via Functional Reformation of Titanium-Oxo Clusters. *J. Am. Chem. Soc.* **2023**, *145*, 6112−6122.
(21) Li, N.; Liu, J.-J.; Sun, J.-W.; Dong, B.-X.; Dong, L.-Z.; Yao, S.-J.; Xin, Z.; Li, S.-L.; Lan, Y.-Q. Calix[8]arene-constructed stable polyoxotitanium clusters for efficient CO_2 photoreduction. *Green Chem.* **2020**, *22*, 5325−5332.
(22) Liu, J.-J.; Li, N.; Sun, J.-W.; Liu, J.; Dong, L.-Z.; Yao, S.-J.; Zhang, L.; Xin, Z.-F.; Shi, J.-W.; Wang, J.-X.; Li, S.-L.; Lan, Y.-Q. Ferrocene-Functionalized Polyoxo-Titanium Cluster for CO_2 Photoreduction. *ACS Catal.* **2021**, *11*, 4510−4519.
(23) Takeda, H.; Cometto, C.; Ishitani, O.; Robert, M. Electrons, Photons, Protons and Earth-Abundant Metal Complexes for Molecular Catalysis of CO2 Reduction. *ACS Catal.* **2017**, *7*, 70−88.
(24) Liu, X.; Inagaki, S.; Gong, J. Heterogeneous Molecular Systems for Photocatalytic CO2 Reduction with Water Oxidation. *Angew. Chem., Int. Ed.* **2016**, *55*, 14924−14950.
(25) Fang, Y.; Wang, X. Photocatalytic CO_2 conversion by polymeric carbon nitrides. *Chem. Commun.* **2018**, *54*, 5674−5687.
(26) Gulati, S.; Vijayan, S.; Mansi; Kumar, S.; Harikumar, B.; Trivedi, M.; Varma, R. S. Recent advances in the application of metal-organic frameworks (MOFs)-based nanocatalysts for direct conversion of carbon dioxide (CO_2) to value-added chemicals. *Coord. Chem. Rev.* **2023**, *474*, No. 214853.
(27) Li, K.; Peng, B.; Peng, T. Recent Advances in Heterogeneous Photocatalytic CO2 Conversion to Solar Fuels. *ACS Catal.* **2016**, *6*, 7485−7527.
(28) Sun, K.; Qian, Y.; Jiang, H.-L. Metal-Organic Frameworks for Photocatalytic Water Splitting and CO_2 Reduction. *Angew. Chem., Int. Ed.* **2023**, *62*, No. e202217565.
(29) Lan, G.; Fan, Y.; Shi, W.; You, E.; Veroneau, S. S.; Lin, W. Biomimetic active sites on monolayered metal−organic frameworks for artificial photosynthesis. *Nat. Catal.* **2022**, *5*, 1006−1018.
(30) Ghosh, A. C.; Legrand, A.; Rajapaksha, R.; Craig, G. A.; Sassoye, C.; Balázs, G.; Farrusseng, D.; Furukawa, S.; Canivet, J.; Wisser, F. M. Rhodium-Based Metal−Organic Polyhedra Assemblies for Selective CO2 Photoreduction. *J. Am. Chem. Soc.* **2022**, *144*, 3626−3636.
(31) Ma, Y.; Wang, X.; Jia, Y.; Chen, X.; Han, H.; Li, C. Titanium Dioxide-Based Nanomaterials for Photocatalytic Fuel Generations. *Chem. Rev.* **2014**, *114*, 9987−10043.
(32) Wang, W.-N.; An, W.-J.; Ramalingam, B.; Mukherjee, S.; Niedzwiedzki, D. M.; Gangopadhyay, S.; Biswas, P. Size and Structure Matter: Enhanced CO2 Photoreduction Efficiency by Size-Resolved Ultrafine Pt Nanoparticles on TiO_2 Single Crystals. *J. Am. Chem. Soc.* **2012**, *134*, 11276−11281.
(33) Yao, S.; He, J.; Gao, F.; Wang, H.; Lin, J.; Bai, Y.; Fang, J.; Zhu, F.; Huang, F.; Wang, M. Highly selective semiconductor photocatalysis for CO2 reduction. *J. Mater. Chem. A.* **2023**, *11*, 12539−12558.
(34) Yu, J.; Low, J.; Xiao, W.; Zhou, P.; Jaroniec, M. Enhanced Photocatalytic CO2-Reduction Activity of Anatase TiO2 by Coexposed {001} and {101} Facets. *J. Am. Chem. Soc.* **2014**, *136*, 8839−8842.
(35) Won, D.-I.; Lee, J.-S.; Ji, J.-M.; Jung, W.-J.; Son, H.-J.; Pac, C.; Kang, S. O. Highly Robust Hybrid Photocatalyst for Carbon Dioxide Reduction: Tuning and Optimization of Catalytic Activities of Dye/TiO_2/Re(I) Organic−Inorganic Ternary Systems. *J. Am. Chem. Soc.* **2015**, *137*, 13679−13690.
(36) Rao, H.; Schmidt, L. C.; Bonin, J.; Robert, M. Visible-light-driven methane formation from CO_2 with a molecular iron catalyst. *Nature* **2017**, *548*, 74−77.
(37) Thoi, V. S.; Kornienko, N.; Margarit, C. G.; Yang, P.; Chang, C. J. Visible-Light Photoredox Catalysis: Selective Reduction of Carbon Dioxide to Carbon Monoxide by a Nickel N-Heterocyclic Carbene−Isoquinoline Complex. *J. Am. Chem. Soc.* **2013**, *135*, 14413−14424.
(38) Wang, S.; Yao, W.; Lin, J.; Ding, Z.; Wang, X. Cobalt Imidazolate Metal−Organic Frameworks Photosplit CO_2 under Mild Reaction Conditions. *Angew. Chem., Int. Ed.* **2014**, *53*, 1034−1038.
(39) Chang, X.; Wang, T.; Gong, J. CO2 photo-reduction: insights into CO2 activation and reaction on surfaces of photocatalysts. *Energy Environ. Sci.* **2016**, *9*, 2177−2196.
(40) Zhang, H.; Wei, J.; Dong, J.; Liu, G.; Shi, L.; An, P.; Zhao, G.; Kong, J.; Wang, X.; Meng, X.; Zhang, J.; Ye, J. Efficient Visible-Light-Driven Carbon Dioxide Reduction by a Single-Atom Implanted Metal−Organic Framework. *Angew. Chem., Int. Ed.* **2016**, *55*, 14310−14314.
(41) Fang, W.-H.; Zhang, L.; Zhang, J. Synthetic strategies, diverse structures and tuneable properties of polyoxo-titanium clusters. *Chem. Soc. Rev.* **2018**, *47*, 404−421.
(42) Zhang, Y.; de Azambuja, F.; Parac-Vogt, T. N. The forgotten chemistry of group(IV) metals: A survey on the synthesis, structure, and properties of discrete Zr(IV), Hf(IV), and Ti(IV) oxo clusters. *Coord. Chem. Rev.* **2021**, *438*, No. 213886.
(43) Zhai, H.-L.; Hou, J.-L.; Luo, C.-Y.; Ma, L.-J.; Zhu, Q.-Y.; Dai, J. Photocurrent and Gelation Properties of Polyphenol-Modified Titanium-Oxo Compounds. *Inorg. Chem.* **2022**, *61*, 13191−13198.
(44) Yang, X.-X.; Yu, W.-D.; Yi, X.-Y.; Liu, C. Accurate Regulating of Visible-Light Absorption in Polyoxotitanate−Calix[8]arene Systems by Ligand Modification. *Inorg. Chem.* **2020**, *59*, 7512−7519.
(45) Dai, L.-F.; Liu, X.-R.; Tian, Y.-Q.; Yi, X.-Y.; Liu, C. Auxiliary Carboxylate-Induced Assembly of Calix[6]arene-Polyoxotitanate Hybrid Systems with Photocatalytic Activity in the Oxidation of Sulfides. *Inorg. Chem.* **2023**, *62*, 6047−6054.

https://doi.org/10.1021/jacs.3c04480
J. Am. Chem. Soc. XXXX, XXX, XXX−XXX

(46) Wang, C.; Wang, S.-J.; Kong, F.-G. Calixarene-Protected Titanium-Oxo Clusters and Their Photocurrent Responses and Photocatalytic Performances. *Inorg. Chem.* **2021**, *60*, 5034−5041.
(47) Xing, T.; Prior, T. J.; Chen, K.; Redshaw, C. Titanium complexes bearing oxa- and azacalix[4, 6]arenes: structural studies and use in the ring opening homo-/co-polymerization of cyclic esters. *Dalton Trans.* **2021**, *50*, 4396−4407.
(48) Tian, Y.-Q.; Cui, Y.-S.; Yu, W.-D.; Xu, C.-Q.; Yi, X.-Y.; Yan, J.; Li, J.; Liu, C. An ultrastable Ti-based metallocalixarene nanocage cluster with photocatalytic amine oxidation activity. *Chem. Commun.* **2022**, *58*, 6028−6031.
(49) Petrella, A. J.; Roberts, N. K.; Raston, C. L.; Thornton-Pett, M.; Lamb, R. N. Titanocene dichloride route to a tetranuclear oxo-bridged monocyclopentadienyl titanium(iv) calix[4]arene complex. *Chem. Commun.* **2003**, *11*, 1238−1239.
(50) Li, N.; Liu, J.; Liu, J.-J.; Dong, L.-Z.; Li, S.-L.; Dong, B.-X.; Kan, Y.-H.; Lan, Y.-Q. Self-Assembly of a Phosphate-Centered Polyoxo-Titanium Cluster: Discovery of the Heteroatom Keggin Family. *Angew. Chem., Int. Ed.* **2019**, *58*, 17260−17264.
(51) Huang, N.-Y.; Shen, J.-Q.; Zhang, X.-W.; Liao, P.-Q.; Zhang, J.-P.; Chen, X.-M. Coupling Ruthenium Bipyridyl and Cobalt Imidazolate Units in a Metal−Organic Framework for an Efficient Photosynthetic Overall Reaction in Diluted CO_2. *J. Am. Chem. Soc.* **2022**, *144*, 8676−8682.
(52) Xu, H.-Q.; Hu, J.; Wang, D.; Li, Z.; Zhang, Q.; Luo, Y.; Yu, S.-H.; Jiang, H.-L. Visible-Light Photoreduction of CO_2 in a Metal−Organic Framework: Boosting Electron−Hole Separation via Electron Trap States. *J. Am. Chem. Soc.* **2015**, *137*, 13440−13443.
(53) Fu, Y.; Sun, D.; Chen, Y.; Huang, R.; Ding, Z.; Fu, X.; Li, Z. An Amine-Functionalized Titanium Metal−Organic Framework Photocatalyst with Visible-Light-Induced Activity for CO_2 Reduction. *Angew. Chem., Int. Ed.* **2012**, *51*, 3364−3367.
(54) Kou, M.; Liu, W.; Wang, Y.; Huang, J.; Chen, Y.; Zhou, Y.; Chen, Y.; Ma, M.; Lei, K.; Xie, H.; Wong, P. K.; Ye, L. Photocatalytic CO_2 conversion over single-atom MoN2 sites of covalent organic framework. *Appl. Catal., B* **2021**, *291*, No. 120146.
(55) Zhou, J.; Li, J.; Kan, L.; Zhang, L.; Huang, Q.; Yan, Y.; Chen, Y.; Liu, J.; Li, S.-L.; Lan, Y.-Q. Linking oxidative and reductive clusters to prepare crystalline porous catalysts for photocatalytic CO_2 reduction with H_2O. *Nat. Commun.* **2022**, *13*, No. 4681.
(56) Gong, S.; Zhu, G.; Wang, R.; Rao, F.; Shi, X.; Gao, J.; Huang, Y.; He, C.; Hojamberdiev, M. Synergistically boosting highly selective CO_2−to−CO photoreduction over BiOCl nanosheets via in-situ formation of surface defects and non-precious metal nanoparticles. *Appl. Catal., B* **2021**, *297*, No. 120413.
(57) Shi, J.-W.; Sun, S.-N.; Liu, J.; Niu, Q.; Dong, L.-Z.; Huang, Q.; Liu, J.-J.; Wang, R.; Xin, Z.; Zhang, D.; Niu, J.; Lan, Y.-Q. Calixarene-Functionalized Stable Bismuth Oxygen Clusters for Specific CO_2-to-HCOOH Electroreduction. *ACS Catal.* **2022**, *12*, 14436−14444.

https://doi.org/10.1021/jacs.3c04480
J. Am. Chem. Soc. XXXX, XXX, XXX−XXX